12
Inverse Dynamics of Flexible Multibodies

Applications of artificial manipulation and robotics are steadily increasing in areas such as: microelectronics, agile space aircraft, vacuum mechatronics, satellite-mounted robots, biomedical sciences, teleoperation, assembly lines, manufacturing, and so forth. As a consequence, more demands are being placed on these systems, such as the need to design and use light and fast arms handling heavy payload with accuracy and low energy consumption. If the various links of a manipulator are to be considered rigid, they must be structurally stiff, and this leads to bulky and massive designs. If speed is not to be sacrificed, powerful and heavy actuators with high energy consumption are in turn required to move these arms. The most natural remedy is to use flexible multibodies with slender links.

The requirement that manipulators and multibody systems be flexible places new demands and challenges in their design, analysis, and control. The flexibility of their members becomes a very important factor that must be considered, so that vibrations are avoided, particularly for position control. In this chapter, concentration will be placed on the inverse dynamics of flexible multibodies. This recently introduced approach (Bayo (1987) and Bayo et al. (1989)) consists of finding the feed-forward torques that need to be applied at the joints so that the end effector can follow a desired trajectory. From the vibration control viewpoint, the inverse dynamics provides an inversion of the system dynamics. This gives the control specialist a strong tool with which he can design stable and robust control laws for the motion control of multibody systems (Paden et al. (1993)).

This chapter begins with the solution of the single-link case where the elastic Coriolis and centrifugal terms are negligible, and algorithms are proposed for the solution of the resulting time invariant system. The algorithms are then extended for the time variant case that includes the Coriolis and centrifugal terms. Solutions in the time and frequency domains are provided. It is clearly shown how the inverse solution is anticipatory; also called *non-causal*, meaning that the actuation precedes the endpoint motion and continues after it has stopped. For the sake of clarity and conciseness, we will concentrate on the planar case, and we will provide indications as to how to proceed with the 3D cases. Simulation examples are given to clarify the meaning of the inverse dynamics.

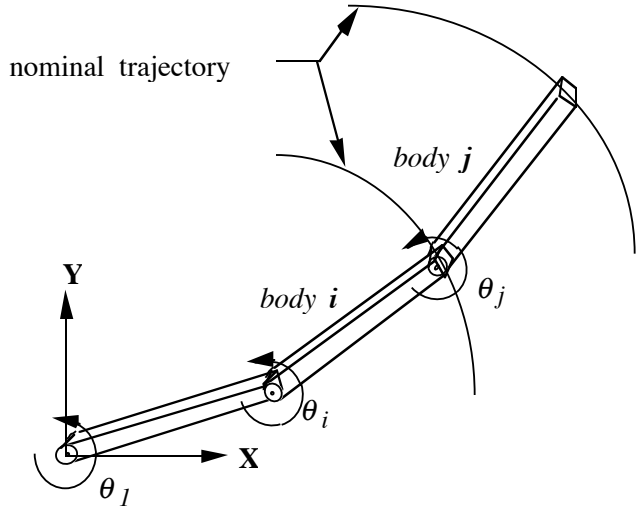

Figure 12.1. Flexible multibody system.

The techniques and methods explained in this chapter are somehow more advanced than those seen in previous chapters. *Non-causal* integration requires that the reader be familiar with the basics of Fourier and Laplace analysis. In this chapter, we deviate from the natural coordinates and use the reference point coordinates instead. This is because the reference point coordinates provide a better setting for the non-causal inversion that the inverse dynamics require.

12.1 Inverse Dynamics Equations for Planar Motion

Consider a general multi-link flexible multibody system (Figure 12.1). The objective is to move the end effector along a given trajectory without overshoot and residual elastic oscillations of the tip. These oscillations are due mainly to the transverse elastic displacements of the links. The longitudinal axial oscillations are negligible because of the much greater rigidity of the links in their axial direction. For the sake of simplicity, the equations will be derived for planar manipulators with revolute joints. The procedure, however, is also valid for general spatial manipulators.

The solution is obtained by first studying an individual link in the chain, coupling the equations of the individual links, and then setting up an iteration scheme that converges to the desired torques and corresponding joint displacements.

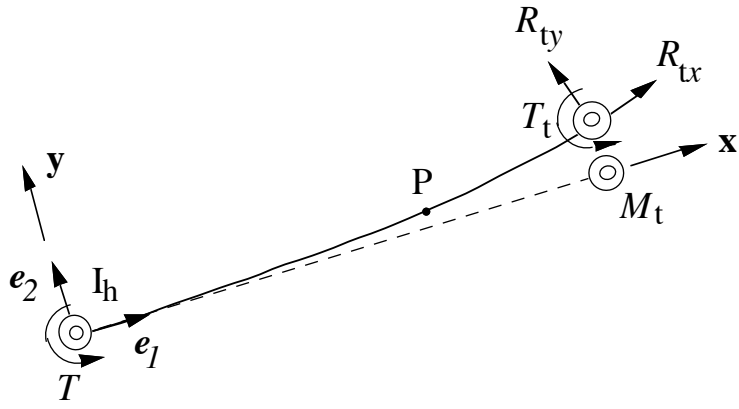

Figure 12.2. Nominal motion (dotted) and elastic deformation (solid) in a flexible body.

12.1.1 Inverse Dynamics Equations of an Individual Link

The individual flexible link depicted in Figure 12.2 forms part of a planar multilink manipulator and has a total length L, mass per unit length $\overline{m}$, moment of inertia I, area A, Young modulus E, shear modulus G, and shear coefficient k. A tip mass of value M_t is attached at one end, and a hub of inertia I_h at the other end. The hub is attached to the actuator.

A point P at a distance x from the center of the hub has undergone elastic deflections of value u_x and u_y and rotation θ. These are defined with respect to a nominal position characterized by the moving frame ($\mathbf{e}_1$, $\mathbf{e}_2$) attached to the hub, that rotates at a specified (nominal) angular velocity and acceleration $\boldsymbol{\omega}_h$ and $\dot{\boldsymbol{\omega}}_h$, respectively. The idea of the inverse dynamics is to force the end of the link to follow the specified (desired) nominal motion. This is an important conceptual difference with the methods of Chapter 11, in which the nominal motion of the moving frame was not specified, because it was actually unknown.

As a consequence of the elastic deflections and rotating nominal motion, the point P is subjected to a total translational acceleration $\mathbf{a}_\mathrm{p}$ and angular acceleration $\dot{\boldsymbol{\omega}}_\mathrm{p}$. Using the principles of relative motion (Greenwood (1988)), the acceleration of the point P can be set in terms of the translation and angular accelerations at the hub, $\mathbf{a}_\mathrm{h}$ and $\dot{\boldsymbol{\omega}}_\mathrm{h}$, angular velocity $\boldsymbol{\omega}_\mathrm{h}$ at the hub, and the relative velocity $\mathbf{v}_\mathrm{rel}$ and acceleration $\mathbf{a}_\mathrm{rel}$ of point P. The latter are due to the elastic deflections u_x and u_y with respect to the moving frame. In vectorial notation:

$$\mathbf{a}_\mathrm{p} = \boldsymbol{\omega}_\mathrm{h} \wedge (\boldsymbol{\omega}_\mathrm{h} \wedge \bar{\mathbf{r}}_\mathrm{p}) + \dot{\boldsymbol{\omega}}_\mathrm{h} \wedge \bar{\mathbf{r}}_\mathrm{p} + 2\, \boldsymbol{\omega}_\mathrm{h} \wedge \mathbf{v}_\mathrm{rel} + \mathbf{a}_\mathrm{h} + \mathbf{a}_\mathrm{rel} \tag{12.1a}$$

$$\dot{\boldsymbol{\omega}}_\mathrm{p} = \dot{\boldsymbol{\omega}}_\mathrm{h} + \ddot{\boldsymbol{\theta}} \tag{12.1b}$$

where $\bar{\mathbf{r}}_\mathrm{P} = (x + u_x)\, \mathbf{e}_1(t) + u_y\, \mathbf{e}_2(t)$ is the position of P after deformation, relative to the hub.

The components of the relative velocity are $\dot{u}_x$ and $\dot{u}_y$. Those of the relative acceleration are $\ddot{u}_x$ and $\ddot{u}_y$. Performing the vectorial operations involved in (12.1) the following components of the accelerations are obtained:

$$\begin{aligned} a_x &= -\omega_h^2 u_x - \dot{\omega}_h u_y - 2\omega_h \dot{u}_y + \ddot{u}_x - \omega_h^2 x + a_{hx} \\ a_y &= -\omega_h^2 u_y + \dot{\omega}_h u_x + 2\omega_h \dot{u}_x + \ddot{u}_y + \dot{\omega}_h x + a_{hy} \\ \dot{\omega}_p &= \dot{\omega}_h + \ddot{\theta} \end{aligned} \tag{12.2}$$

Using the Timoshenko beam theory which includes the effects of shear deformation and rotatory inertia, the principle of virtual displacements (Chapter 4) can be used directly to set up the equations of motion:

$$\begin{aligned} &\int_0^L \left[\overline{m}\, a_x\, \delta u_x + \overline{m}\, a_y\, \delta u_y + \overline{m}\, \eta^2\, \dot{\omega}_p \delta\theta\right] dx + I_h(\dot{\omega}_h + \ddot{\theta}_h)\delta\theta_h + M_t\, a_t\, \delta u_t + \\ &+ \int_0^L \left[EA\, u_x'\, \delta u_x' + EI\, \theta'\delta\theta' + GAk\,(\theta - u_y')\,\delta(\theta - u_y')\right] dx = \\ &= T\delta\theta_h + R_{ty}\,\delta u_{ty} + R_{tx}\,\delta u_{tx} + T\delta\theta_t \end{aligned} \tag{12.3}$$

where η is the radius of gyration of the section. The subscripts h and t indicate hub and tip, respectively. The symbol (') indicates derivative with respect to the spatial variable, and δu_x, δu_y, and $\delta\theta$ represent a set of virtual elastic displacements. T is the unknown torque to be applied at the hub, so that the prescribed tip motion is obtained. R_{ty} , R_{tx}, and T_t are the reaction forces and the torque at the tip that comes from the next link in the chain (See Figure 12.2). Note that the acceleration at the hub is decomposed into $\dot{\omega}_h$ and $\dot{\omega}_h$. The first is the nominal acceleration, and the second is the acceleration due to the elastic deflections. Also observe that the reactions at the hub do not have any effect on the total virtual work. This assumption is met by imposing the constraint that the hub move along the nominal path without any elastic deformations (See Figure 12.1). As shown later in the discussion, this condition is enforced in each of the links to compute the inverse dynamic torques. Substituting equation (12.2) into (12.3), one can obtain:

$$\begin{aligned} &\int_0^L [\overline{m}\,\ddot{u}_x\delta u_x + \overline{m}\,\ddot{u}_y\delta u_y + \overline{m}\,\eta^2\,\ddot{\theta}\delta\theta]\,dx + \int_0^L [2\overline{m}\,\omega_h\,(\dot{u}_x\,\delta u_y - \dot{u}_y\,\delta u_x)\,]\,dx + \\ &+ \int_0^L [\,\overline{m}\,\omega_h^2(-u_x\,\delta u_x - u_y\,\delta u_y) + \dot{\omega}_h\,\overline{m}\,(u_x\,\delta u_y - u_y\,\delta u_x]\,dx + \\ &+ I_h(\dot{\omega}_h + \ddot{\theta}_h)\,\delta\theta_h + M_t\,a_t\delta u_t + \int_0^L [EI\,\theta'\delta\theta' + GAk(\theta - u_y')\,\delta(\theta - u_y') + EAu_x'\,\delta u_x']\,dx = \\ &= T\,\delta\theta_h + R_{ty}\delta u_{ty} + R_{tx}\delta u_{tx} + T_t\delta\theta_t - \int_0^L [-\overline{m}\omega_h^2\,x\delta u_x + \overline{m}\dot{\omega}_h\,x\,\delta u_y + \overline{m}\eta^2\dot{\omega}_h\delta\theta]dx \end{aligned} \tag{12.4}$$

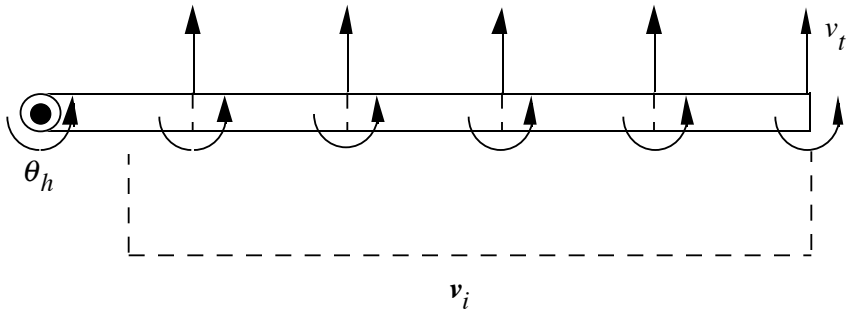

Figure 12.3. Finite element partition in the body.

The first integral on the LHS corresponds to the internal virtual work done by the inertial forces including the rotatory inertia. The second integral term represents the work done by the Coriolis forces. The third integral corresponds to the centrifugal and tangential forces due to the rotating frame. This last effect also produces additional forcing terms that are represented in the RHS of the equation. The fourth integral corresponds to the virtual work done by the internal axial and shear forces and bending moments.

The displacement field of equation (12.3) can be discretized using the finite element or assumed mode method under *pin-free* boundary conditions (Figure 12.3). A set of interpolation functions are defined within each body:

$$u_x(x,t) = \sum_1^n H_i(x)\, u_x^i(t), \quad u_y(x,t) = \sum_1^n H_i(x)\, u_y^i(t), \quad \theta(x,t) = \sum_1^n H_i(x)\, \theta^i(t) \qquad (12.5)$$

where H_i are the interpolation functions; u_x^i, u_y^i, and θ^i indicate the nodal or generalized deflections.

Substituting equations (12.5) in the virtual work expression (12.4), and following standard procedures for the formation and assemblage of element matrices (Bathe 1982), the equations of motion of the link may be expressed by a set of time varying differential equations in the form

$$\mathbf{M}\,\ddot{\mathbf{v}} + \left[\mathbf{C} + \mathbf{C_c}(\omega_\mathrm{h})\right]\dot{\mathbf{v}} + \left[\mathbf{K} + \mathbf{K_c}(\omega_\mathrm{h},\, \dot{\omega}_\mathrm{h})\right]\mathbf{v} = \mathbf{T} - \mathbf{Q}(\omega_\mathrm{h},\, \dot{\omega}_\mathrm{h}) \qquad (12.6)$$

where $\mathbf{M}$ and $\mathbf{K}$ are the conventional finite element (or assumed mode) mass and stiffness matrices, respectively. $\mathbf{C_c}$ and $\mathbf{K_c}$ are the time varying Coriolis and centrifugal stiffness matrices that depend on the nominal angular velocity ω_h and acceleration $\dot{\omega}_\mathrm{h}$ of the link. Matrix $\mathbf{C}$ has been added to represent the internal viscous damping of the material. Vector $\mathbf{T}$ contains one non-zero term only, and that is the unknown torque at the hub. Finally, $\mathbf{Q}$ contains the reactions and the torque at the end of the link and the known forces produced by the rotating frame effect. A detailed description of these matrices for a Timoshenko beam finite element is given in the Appendix.

12.1.2 Solution of the Inverse Dynamics for an Individual Link

The set of equations (12.6) may be partitioned as follows:

$$\mathbf{M}\begin{bmatrix}\ddot{\theta}_h\\ \ddot{\mathbf{v}}_i\\ \ddot{v}_t\end{bmatrix} + [\mathbf{C} + \mathbf{C}(\omega_h)]\begin{bmatrix}\dot{\theta}_h\\ \dot{\mathbf{v}}_i\\ \dot{v}_t\end{bmatrix} + [\mathbf{K} + \mathbf{K}_c(\dot{\omega}_h, \omega_h)]\begin{bmatrix}\theta_h\\ \mathbf{v}_i\\ v_t\end{bmatrix} = \begin{bmatrix}1\\0\\0\end{bmatrix} T - \begin{bmatrix}Q_h\\ \mathbf{Q}_i\\ Q_t\end{bmatrix} \quad (12.7)$$

where θ_h is the rotation at the hub, v_t is the elastic deflection of the end point, and $\mathbf{v}_i$ is the vector containing all the other internal finite element degrees of freedom such as displacements and rotations of the nodal points, as shown in Figure 12.3. The force vector $\mathbf{Q}$ is partitioned in the same manner.

The solution of equations (12.7) for a specified nominal motion, defined by ω_h and $\dot{\omega}_h$, and a set of external forces applied to the link, constitutes the forward dynamic problem. This simply requires the numerical integration of a set of time variant ODEs for which techniques are readily available (See Chapter 7). A problem of different and more complicated nature is the inverse dynamics. This problem is to find the torque T that will ensure that the endpoint will move according to a specified trajectory avoiding any possible oscillations and deviations from the path. The problem can be quantitatively stated as the finding of $T(t)$ in equation (12.7) under the condition that elastic normal deflection at the tip $v_t(t)$ be zero.

12.1.2.1 The Time Invariant Case

Under low nominal speeds of operations, the elastic Coriolis and centrifugal terms acting on the LHS of equation (12.7) become insignificant and are customarily neglected. An example will be shown later which clearly illustrates this assumption. Consequently, equation (12.6) becomes

$$\mathbf{M}\,\ddot{\mathbf{v}} + \mathbf{C}\,\dot{\mathbf{v}} + \mathbf{K}\,\mathbf{v} = \mathbf{T} - \mathbf{Q}(\omega_h, \dot{\omega}_h) \quad (12.8)$$

Observe that the force vector $\mathbf{Q}$ in the RHS of (12.8) contains the external Coriolis and centrifugal forcing terms due to the rigid body motion which are not neglected (See Appendix).

Direct integration in the time domain. The inverse dynamics is, in the classical sense, an ill-posed problem, because its solution does not depend continuously on the data. The intention of this section is to briefly describe that a standard integration in the time domain leads to an unbounded (thus unstable) solution and that the *unique stable solution is found to be non-causal*. Actuation is required before the endpoint has started to move as well as after the endpoint has stopped. After a first glance at equation (12.8) one may be tempted to partition the system of equations as follows:

$$\begin{bmatrix}\mathbf{M}_{11}\ m_{12}\\ \mathbf{M}_{21}\,\mathbf{M}_{22}\end{bmatrix}\begin{bmatrix}\ddot{\theta}_h\\ \ddot{\mathbf{v}}_i\\ \ddot{v}_t\end{bmatrix} + \begin{bmatrix}\mathbf{C}_{11}\ c_{12}\\ \mathbf{C}_{21}\,\mathbf{C}_{22}\end{bmatrix}\begin{bmatrix}\dot{\theta}_h\\ \dot{\mathbf{v}}_i\\ \dot{v}_t\end{bmatrix} + \begin{bmatrix}\mathbf{K}_{11}\ k_{12}\\ \mathbf{K}_{21}\,\mathbf{K}_{22}\end{bmatrix}\begin{bmatrix}\theta_h\\ \mathbf{v}_i\\ v_t\end{bmatrix} = \begin{bmatrix}1\\0\\0\end{bmatrix} T - \begin{bmatrix}Q_h(t)\\ \mathbf{Q}_i(t)\\ Q_t(t)\end{bmatrix} \quad (12.9)$$

where for a system with n degrees of freedom (n equations): $\mathbf{M}_{11}$, $\mathbf{C}_{11}$, and $\mathbf{K}_{11}$ are *1×(n–1)* row vectors; m_{12}, c_{12} and k_{12} are *(1×1)* elements; $\mathbf{M}_{21}$, $\mathbf{C}_{21}$, and $\mathbf{K}_{21}$ are *(n–1)×(n–1)* matrices; and, $\mathbf{M}_{22}$, $\mathbf{C}_{22}$, and $\mathbf{K}_{22}$ are *(n–1)×1* column vectors. Collecting the $v_t(t)$ dependent known terms on the right-hand side, the last *n–1* equations of (12.9) can be rewritten as:

$$\mathbf{M}_{11}\begin{bmatrix}\ddot{\theta}_h\\ \ddot{\mathbf{v}}_i\end{bmatrix} + m_{12}\,\ddot{v}_t + \mathbf{C}_{11}\begin{bmatrix}\dot{\theta}_h\\ \dot{\mathbf{v}}_i\end{bmatrix} + c_{12}\,\dot{v}_t + \mathbf{K}_{11}\begin{bmatrix}\theta_h\\ \mathbf{v}_i\end{bmatrix} + k_{12}\,v_t = T(t) - Q_h(t) \qquad (12.10)$$

while the first equation of (12.9) is

$$\mathbf{M}_{11}\begin{bmatrix}\ddot{\theta}_h\\ \ddot{\mathbf{v}}_i\end{bmatrix} + m_{12}\,\ddot{v}_t + \mathbf{C}_{11}\begin{bmatrix}\dot{\theta}_h\\ \dot{\mathbf{v}}_i\end{bmatrix} + c_{12}\,\dot{v}_t + \mathbf{K}_{11}\begin{bmatrix}\theta_h\\ \mathbf{v}_i\end{bmatrix} + k_{12}\,v_t = T(t) - Q_h(t) \qquad (12.11)$$

In principle, given initial conditions for $\theta_h(t=0)$ and $v_i(t=0)$, equation (12.10) may be integrated to yield $\theta_h(t)$ and $v_i(t)$ (inverse kinematics). Then, substitution of $\theta_h(t)$ and $v_i(t)$ into equation (12.11) would yield the required actuating torque $T(t)$ (inverse dynamics). However, this simple approach yields an *unbounded* and thus unacceptable solution, which does include a time delay between the actuation and the response at the endpoint.

In order to clarify this point, let the beginning of the prescribed tip motion be at time zero; so that $v_i(t)$ is zero for $t < 0$, and let the arm be initially at rest. Since the elastic waves in a solid have a finite speed of propagation, intuition dictates that in the case of a flexible arm, the torque must be applied before the tip starts moving; that is, it must be non-zero before $t=0$. This time anticipation is necessary for the actuation to reach the end of the arm. Using a term customarily used in control theory, the desired torque should be *non-causal*. As a consequence, if standard numerical integration of ODEs for initial value problems is carried out, no time anticipation would be present, and the resulting torque becomes unbounded. From a control point of view it can be said that this way of proceeding leads to a *causal* inverse which, in the case of a non-minimum phase problem such as the one at hand, is always unbounded and thus unstable. This important point is addressed in detail in Moulin (1989), and Moulin and Bayo (1991).

Allowing for this time delay, let the actuation begin at some negative time τ with the arm initially at rest and initial conditions equal to zero. Now, over $[\tau, 0]$ $v_t(t)$ is identically zero, and the unique solution of equation (12.9) with zero initial conditions and zero terms on the right-hand side will be $\theta_h(t)=0$ and $\mathbf{v}_i(t)=0$. Substitution of $\theta_h(t)$ and $\mathbf{v}_i(t)$ into equation (12.11) leads again to $T(t) = 0$ over $[\tau, 0]$. Hence, the torque resulting from this approach is always zero before the tip starts moving and does not lead to the desired time anticipatory non-causal inverse dynamic solution described above. The delay effect does not appear, regardless of the value of the time τ introduced, and the resulting torque becomes unbounded.

In summary, the inverse dynamic equations need to be solved by means of an integration process that will yield the time delay between actuation and response. The fact that the stable solution is *non-causal* in that it starts at negative time

and extends to future time precludes standard time domain initial value ODE solvers from obtaining the proper solution. We will show in the next sections how this problem can be circumvented by solving the inverse dynamics in the *frequency domain* using the Fourier transform, or in the *time domain* using the bilateral Laplace transform.

Solution in the frequency domain. The frequency domain approach captures the desired time delay between actuation and response, because the initial and end conditions are imposed at -∞ and +∞, respectively. The system of equations (12.8) can be transformed by means of the fast Fourier transform (FFT) (Newland (1984)) into a set of algebraic equations with complex entries. The frequency associated with each of the Fourier pairs is equal to $\overline{w}_i = (2\pi/\Pi)\, i$, where Π is the total time interval considered for the motion of the system and i is the number of the Fourier pair. For a particular frequency $\overline{w}$, equation (2) becomes

$$\left[\mathbf{M} + \frac{1}{j\,\overline{w}}\,\mathbf{C} - \frac{1}{\overline{w}^2}\,\mathbf{K}\right] \begin{Bmatrix} \hat{\ddot{v}}_{\mathrm{h}} \\ \hat{\ddot{\mathbf{v}}}_{\mathrm{i}} \\ \hat{\ddot{v}}_{\mathrm{t}} \end{Bmatrix} = \begin{Bmatrix} \hat{T}\,(\overline{w}) \\ 0 \\ 0 \end{Bmatrix} - \begin{Bmatrix} \hat{Q}_{\mathrm{h}} \\ \hat{\mathbf{Q}}_{\mathrm{i}} \\ \hat{Q}_{\mathrm{t}} \end{Bmatrix} \tag{12.12}$$

where the caret stands for the Fourier transform, and **Q** represents all the known forcing terms. Equation (12.12) may be expressed in simplified notation as

$$\mathbf{H}\,\hat{\ddot{\mathbf{v}}} = \mathbf{I}\,\hat{T}\,(\overline{w}) - \hat{\mathbf{Q}} \tag{12.13}$$

The transfer matrix **H** is a complex non-singular symmetric matrix except for $\overline{w} = 0$ for which it is not defined. However, the zero frequency represents the rigid body motion. Therefore, the corresponding component of the torque can be obtained by simply applying equilibrium of the moments produced by all the external forces about the origin of the link. For the Fourier pairs with $\overline{w} \neq 0$, $\hat{T}\,(\overline{w})$ may be obtained by solving (12.13) for each frequency as follows:

$$\begin{Bmatrix} \hat{\ddot{v}}_{\mathrm{h}} \\ \hat{\ddot{\mathbf{v}}}_{\mathrm{i}} \\ \hat{\ddot{v}}_{\mathrm{t}} \end{Bmatrix} = \begin{bmatrix} G_{\mathrm{hh}} & \mathbf{G}_{\mathrm{hi}} & G_{\mathrm{ht}} \\ \mathbf{G}_{\mathrm{ih}} & \mathbf{G}_{\mathrm{ii}} & \mathbf{G}_{\mathrm{it}} \\ G_{\mathrm{th}} & \mathbf{G}_{\mathrm{ti}} & G_{\mathrm{tt}} \end{bmatrix} \left(\begin{Bmatrix} \hat{T}\,(\omega) \\ 0 \\ 0 \end{Bmatrix} - \begin{Bmatrix} \hat{Q}_{\mathrm{h}} \\ \hat{\mathbf{Q}}_{\mathrm{i}} \\ \hat{Q}_{\mathrm{t}} \end{Bmatrix} \right) \tag{12.14}$$

where **G** is the inverse of the complex transfer matrix **H**. From (12.14), it is obvious that

$$\hat{\ddot{v}}_{\mathrm{t}} = G_{\mathrm{th}}\,\hat{T}\,(\overline{w}) - G_{\mathrm{th}}\,\hat{Q}_{\mathrm{h}} - \mathbf{G}_{\mathrm{ti}}\,\hat{\mathbf{Q}}_{\mathrm{i}} - G_{\mathrm{tt}}\,\hat{Q}_{\mathrm{t}} \tag{12.15}$$

Equation (12.15) may now be solved for the required torque T under the condition that $v_t = 0$:

$$\hat{T}\,(\overline{w}) = G_{\mathrm{th}}^{-1}\,\left(G_{\mathrm{th}}\,\hat{Q}_{\mathrm{h}} + \mathbf{G}_{\mathrm{ti}}\,\hat{\mathbf{Q}}_{\mathrm{i}} + G_{\mathrm{tt}}\,\hat{Q}_{\mathrm{t}}\right) \tag{12.16}$$

The values of the torque $T(t)$ are obtained through the application of the inverse discrete Fourier transform. The joint angles and velocities that will yield the desired endpoint motion (inverse kinematics), and which are used for control purposes (Paden et al. (1993)), can be obtained in the time domain by a forward

integration of equation (12.8). Since the forces **Q** are linear functions of the nominal accelerations, equation (12.16) also leads to an expression for the transfer function between the torque T and the endpoint acceleration. This transfer function contains poles in the right half-plane; thus characterizing this non-minimum phase system.

By using the frequency domain, the initial and final conditions are imposed at -∞ and +∞. This leads to an inverse dynamics torque that shows the above-mentioned time anticipation with respect to the endpoint motion (See example below); thus providing the *non-causal* inverse to this non-minimum phase problem. A formal explanation of this issue is given in Moulin (1989), and Moulin and Bayo (1991).

The following algorithm summarizes the steps necessary for the inverse dynamics and kinematics of a single-link arm in the frequency domain:

Algorithm 12-1

1. Define the rigid nominal motion, ω_h and $\dot{\omega}_h$.
2. Evaluate the forcing terms Q_h, $\mathbf{Q}_i$, and Q_t which depend on ω_h and $\dot{\omega}_h$.
3. Apply the fast Fourier transform to the forcing terms.
4. Solve for the torque $\widehat{T}(\overline{w})$ in the frequency domain using equation (12.16). This involves the solution of a set of algebraic linear complex equations.
5. Obtain *T(t)* through the inverse discrete Fourier transform.
6. Perform a forward time integration of equation (12.8) to obtain the joint angles and velocities (inverse kinematics).

Stable integration in the time domain. From the above observation that in order to obtain a stable inverse that includes the delay between the actuation and response, the integration process needs to be carried out from -∞ to +∞. The equivalent of equation (12.16) in the time domain is

$$T(t) = \int_{-\infty}^{\infty} \left(h_{th}(t-\tau)\ Q_h(\tau) + \mathbf{h}_{ti}(t-\tau)\ \mathbf{Q}_i(\tau) + h_{tt}(t-\tau)\ Q_t(\tau) \right) d\tau \qquad (12.17)$$

where h_{th}, $\mathbf{h}_{ti}$, and h_{tt} are the impulse response functions that correspond to the transfer functions defined in (12.16). The former are the inverse Fourier transforms of the latter.

Since there is no complex algebra involved, the integration in the time domain will in general be faster than that in the frequency domain. In addition, since the impulse response functions depend only on the physical characteristics of the link, they can be computed off-line. The only on-line computations involved consequently to obtain the torque *T(t)* will be the evaluation of the integral (12.17).

It should be observed that equation (12.17) differs from the familiar Duhamel integral:

$$y(t) = \int_0^t h(t-\tau)\ i(\tau)\, d\tau \qquad (12.18)$$

Figure 12.4. Typical tip-to-hub impulse response function of a flexible body.

relating the input $i(t)$ to the output $y(t)$ of a linear system with impulse response function $h(t)$ by the bounds of integration.

Equation (12.18) which is typical of a causal response is valid when the input $i(\tau)$ and the response function $h(t)$ are zero for $\tau < 0$. The condition on $h(\tau)$ states that there is no output before there is an input, in other words the system is *causal*. In the inverse dynamics problem, the input is formally the tip acceleration profile, and the output is formally the actuating torque. As mentioned above, there is a delay in the forward problem between hub torque actuation and tip response. Therefore in the inverse problem, the torque must be applied before the tip starts moving. The inverse is *non-causal*. For a non-causal system, the impulse response functions in (12.17) are not identically zero for negative time. Figure 12.4 shows a typical impulse response function for inverse dynamics. The convolution integral of (12.17) cannot be reduced to that of (12.18).

The use of equation (12.17) hinges on the availability of the impulse response functions. This can be obtained in the following manner: if the input α_h is a Dirac delta function at time τ, then the output $T(t)$ is the impulse response function translated by τ. One way of obtaining $h_i(t)$ numerically is to use equation (12.16) with an approximation of a delta function for $\dot{\omega}_{\mathrm{h}}$. Having computed the impulse response functions, we now turn to the evaluation of the convolution integral defined by (12.17). This equation can be evaluated at discrete time intervals of length Δt, using a suitable composite integration rule.

The following paragraph summarizes the steps involved in the inverse dynamics integration in the time domain:

Algorithm 12-2

1. Define the rigid nominal motion: ω_h and $\dot{\omega}_h$.
2. Evaluate the impulse response functions.
3. Calculate the forcing terms F_h, $\mathbf{F}_i$, and F_t which depend on ω_h and $\dot{\omega}_h$.
4. Solve for the torque *T(t)* by means of the convolution integrals (12.17).
5. Perform a forward time integration of equation (12.8) to obtain the joint angles and velocities (inverse kinematics).

This algorithm leads to a very fast computation of the inverse dynamics and allows one to obtain real time response (Bayo and Moulin (1989a)). Another efficient time domain approach consists of decomposing the transfer function into its causal and non-causal components (Kwon and Book (1990)).

12.1.2.2 The Time Varying Case

In case the manipulator undergoes a fast motion and one desires to include the elastic Coriolis and centrifugal terms, the solution for the torque *T(t)* can still be found in either the frequency or time domains by means of an iteration procedure. In order to set up the iterative process, equation (12.6) may be restated as follows:

$$\mathbf{M}\,\ddot{\mathbf{v}} + \mathbf{C}\,\dot{\mathbf{v}} + \mathbf{K}\,\mathbf{v} = \mathbf{l}\,T - \mathbf{Q}(\dot{\omega}_h,\,\omega_h) - \mathbf{C}_c(\omega_h)\,\dot{\mathbf{v}} - \mathbf{K}_c(\dot{\omega}_h,\,\omega_h)\,\mathbf{v} \qquad (12.19)$$

where all the time invariant terms have been left in the LHS of the equation and the time varying ones have been collected on the RHS. The vector $\mathbf{l}$ contains a unit value for the degree of freedom corresponding to the hub rotation and zero for the rest, as shown in equation (12.7).

The iteration process is initiated by solving equation (12.19) for the unknown torque *T*, using either the frequency or time domain procedures described above. The first iteration is done in the absence of the last two terms involving $\mathbf{C}_c$ and $\mathbf{K}_c$ in the RHS and yields a displacement vector $\mathbf{v}^1(t)$ which in turn will be used to compute the last two terms in (12.19). The process is then repeated with the new force vector under the constraint that $v_t(t)=0$. The iteration procedure may be stopped, when the norm $\|\mathbf{v}^i - \mathbf{v}^{i-1}\|$ for the solution of two consecutive iterations is smaller than a prescribed tolerance. A formal proof of convergence of this algorithm is given by Moulin et al. (1992). The experience of the authors in all the cases analyzed reveals that unless the accelerations and velocities are large, the terms involving $\mathbf{K}_c$ and $\mathbf{C}_c$ are insignificant, and this iterative procedure can be neglected. Also and most importantly, when the speeds of operations are large, not only the Coriolis and centrifugal terms need be included but also the nonlinear geometric stiffening effects (Bayo and Moulin (1989b)).

Algorithm 12-3

1. Define the rigid nominal motion: ω_h and $\dot{\omega}_h$.
2. Evaluate the forcing terms on the RHS of (12.19) that depend on ω_h, $\dot{\omega}_h$, $\mathbf{v}$, and $\dot{\mathbf{v}}$.
3. Apply the fast Fourier transform to the forcing terms.
4. Solve for the torque $\widehat{T}(\overline{w})$ in the frequency or time domains.
5. Add $T(t)$ to the forces on the RHS of equation (12.19) and perform a forward integration to obtain $\mathbf{v}(t)$ (inverse kinematics).
6. Check convergence. If convergence is obtained, stop; otherwise go to step 2.

12.2 Recursive Inverse Dynamics for Open-Chain Configurations

In this section, the procedure outlined above for the inverse dynamics of the single-link is extended in a recursive manner for multi-link open-chain configurations. These cases can be decomposed into a series of individual links that can be analyzed recursively. This analysis is similar to that used in the previous section.

12.2.1 The Planar Open-Chain Case

Similar to the single-link case, the solution process for an open-chain robot is started by defining the nominal motion consisting of the inverse kinematics of the robot as if it were rigid and characterized by the θ_h, ω_h, and $\dot{\omega}_h$ of each individual link. A difference with respect to the single link arises from the fact that an intermediate link in the chain contains reaction forces at its endpoint. These forces come from the next distal link and are to be added to those arising from the moving frame effect to form the forcing vector $\mathbf{Q}$ in equation (12.19). The solution of equation (12.19) for the desired torque requires that these reaction forces contained in the force vector $\mathbf{Q}$ be known in each link.

In the open-chain case this difficulty can be easily overcome by starting the inverse dynamics with the last link, since in this case there are no link reaction forces at its end. Once the torque for the last link has been obtained under the condition that the elastic displacement at the tip is zero, the next step is to compute the reactions at the hub which will be transmitted to the previous link in the chain. These reactions may be obtained simply by equilibrium considerations. The procedure continues with the next link in the chain in the same manner as before. Reaction forces are present and therefore included. This process is conceptually similar to the recursive Newton-Euler scheme for inverse dynamics of rigid manipulators.

The method continues with the rest of the links, until the torque on the first link is determined. This way of proceeding assures that the end of each link

moves along the desired nominal trajectory without oscillating from it, as shown in Figure 12.1. Once the torques T have been obtained, the motions at any point of the links specified by $\mathbf{v}_i$ or the angles θ_h (inverse kinematics) follow from equation (12.6) by a direct analysis. The basic steps involved in the process are summarized as follows:

Algorithm 12-4

1. Define the nominal motion consisting of inverse kinematics of the system considered rigid.
2. For each link j starting from the last in the chain:
   a) Compute the torque T^j imposing $v^j_{tip}=0$ and obtain $\mathbf{v}$(t) (inverse kinematics) following the single-link time-varying approach.
   b) Compute the link reaction forces R^j from equilibrium.

12.2.2 The Spatial Open-Chain Case

In the case of spatial manipulators with elastic properties in all directions, the elastic displacements contained in the plane defined by the joint axis and the tip of the link cannot be controlled by only one joint torque. These elastic displacements will influence the motions of subsequent links, introducing perturbations in their nominal motion. The nominal position of each link will be modified by the elastic displacements at the end of the previous link as follows:

$$\mathbf{r}^i_n = \mathbf{r}^{i-1}_n - \mathbf{v}_{tip} \tag{12.20}$$

where $\boldsymbol{r}_n$ is a vector describing the nominal position and orientation of the link, $\mathbf{v}_{tip}$ indicates the elastic deformations at the end of the previous link, and "i" is the iteration number. The steps described above for the open- and closed-chain will have to be repeated introducing the displacement corrections, starting with the last link. Assuming that the elastic deformations are small compared to the overall nominal motions, the process should converge rapidly.

According to the authors' experience, the recursive procedure described in the previous section is the most suitable for open-chain configurations in which the elastic deflections on the proximal links does not affect the overall motion of the distal links. Such is the case in the planar open-chain case or in spatial manipulators that are designed with large stiffness in the plane defined by the joint axis and the endpoint of the link; so that the corresponding elastic displacements are negligible. If this is not the case, the recursive procedure demands an iteration process to account for those perturbations, and the inverse dynamics for each link needs to be repeated until convergence. Non-recursive approaches are more suitable and efficient under these circumstances, and we will see them in the next section. Other special recursive methods that avoid the need to iterate are currently being developed in this exciting area of research (Ledesma and Bayo (1992b)).

12.3 Non-Recursive Inverse Dynamics

The methods of this section are due to R. Ledesma and E. Bayo.

We presented in the previous section a recursive procedure for the inverse dynamics that relied on a pinned-free finite element or assumed mode model of a flexible beam, and the equation for the inverse dynamics torque was formulated by imposing the condition, that the transverse deformation of the free end of each link be zero throughout the motion. The recursive procedure is suitable for open-chain but not for closed-chain configurations.

In this section, we describe a non-recursive approach to solve the general planar inverse dynamics and kinematics, that has been introduced by Ledesma and Bayo (1992a). For the sake of simplicity, we will not describe herein the more general non-recursive procedure for spatial flexible multibodies which is presented in Ledesma and Bayo (1993). Compared to the recursive procedure, this non-recursive approach is more systematic and general and becomes the only choice, when closed-chain systems are encountered. The finite element model of the elastic links now has *pinned-pinned* boundary conditions. This allows one to express the end effector trajectory in terms of the rigid body coordinates only. In addition it leads to a simplified form of the inverse kinematics equations. Once these are solved, the equations of motion give an explicit expression for the inverse dynamics torque.

The starting point is the equation for the forward dynamics (11.33) that was developed in Section 11.2. In partitioned form, this equation may be written as

$$\begin{bmatrix} \mathbf{m}_{RR} & \mathbf{m}_{R\theta} & \mathbf{m}_{Rf} \\ \mathbf{m}_{\theta R} & \mathbf{m}_{\theta\theta} & \mathbf{m}_{\theta f} \\ \mathbf{m}_{fR} & \mathbf{m}_{f\theta} & \mathbf{m}_{ff} \end{bmatrix} \begin{Bmatrix} \ddot{\mathbf{R}} \\ \ddot{\boldsymbol{\theta}} \\ \ddot{\mathbf{q}}_f \end{Bmatrix} + \begin{bmatrix} 0 & 0 & 0 \\ 0 & 0 & 0 \\ 0 & 0 & \mathbf{c}_{ff} \end{bmatrix} \begin{Bmatrix} \dot{\mathbf{R}} \\ \dot{\boldsymbol{\theta}} \\ \dot{\mathbf{q}}_f \end{Bmatrix} + \begin{bmatrix} 0 & 0 & 0 \\ 0 & 0 & 0 \\ 0 & 0 & \mathbf{k}_{ff} \end{bmatrix} \begin{Bmatrix} \mathbf{R} \\ \boldsymbol{\theta} \\ \mathbf{q}_f \end{Bmatrix} + \begin{bmatrix} \boldsymbol{\Phi}_R^T \\ \boldsymbol{\Phi}_\theta^T \\ \boldsymbol{\Phi}_{\mathbf{q}_f}^T \end{bmatrix} \boldsymbol{\lambda} = \begin{bmatrix} \mathbf{Q}_{eR} \\ \mathbf{Q}_{e\theta} \\ \mathbf{Q}_{ef} \end{bmatrix} + \begin{bmatrix} \mathbf{Q}_{vR} \\ \mathbf{Q}_{v\theta} \\ \mathbf{Q}_{vf} \end{bmatrix} \tag{12.21}$$

where, as shown in Figure 12.5, $\mathbf{R}$ represents the Cartesian components of the origins of all the body axes with respect to the inertial frame and $\boldsymbol{\theta}$ are the angles of rotation of the body axes. These are the coordinates that define the rigid body motion namely $\mathbf{q}_r = [\mathbf{R}, \boldsymbol{\theta}]^{\mathrm{T}}$. The term $\mathbf{Q}_e$ represents the external loads, and $\mathbf{Q}_v$ the quadratic velocity terms. The second set of equations in (12.21) can be rearranged to express the externally applied joint forces as

$$\mathbf{Q}_{e\theta} = \mathbf{m}_{\theta R}\ddot{\mathbf{R}} + \mathbf{m}_{\theta\theta}\ddot{\boldsymbol{\theta}} + \mathbf{m}_{\theta f}\ddot{\mathbf{q}}_f + \boldsymbol{\Phi}_\theta^{\mathrm{T}}\boldsymbol{\lambda} - \mathbf{Q}_{v\theta} \tag{12.22}$$

Equation (12.22) constitutes the inverse dynamics equation that yields the joint forces (torques) necessary for the endpoint or any other control point to follow a prescribed trajectory. In order to obtain $\mathbf{Q}_{e\theta}$ the nodal acceleration vector $\ddot{\mathbf{q}}_f$ is needed. This vector can be obtained from the third set of equations in (12.21) which may be written as

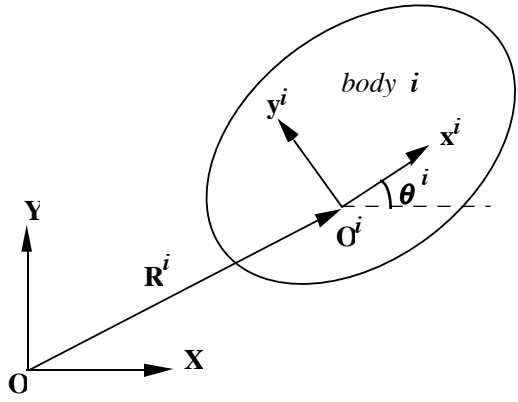

Figure 12.5. Reference frame for a planar flexible body.

$$\mathbf{m}_{ff}\ddot{\mathbf{q}}_f + \mathbf{c}_{ff}\dot{\mathbf{q}}_f + \mathbf{k}_{ff}\mathbf{q}_f = \mathbf{Q}_{ef} + \mathbf{Q}_{vf} - \mathbf{m}_{fR}\ddot{\mathbf{R}} - \mathbf{m}_{f\theta}\ddot{\boldsymbol{\theta}} - \boldsymbol{\Phi}_f^{\mathrm{T}}\boldsymbol{\lambda} \tag{12.23}$$

The vector of applied nodal forces $\mathbf{Q}_{ef}$ can be expressed in terms of the externally applied torques through the following mapping:

$$\mathbf{Q}_{ef} = \mathbf{G}_e\,\mathbf{Q}_{e\theta} \tag{12.24}$$

where in the planar case the matrix $\mathbf{G}_f$ is a constant Boolean matrix which maps the externally applied torques to the vector of externally applied nodal forces. For example, in the open-chain planar multibody system shown in Figure 12.6, the Boolean matrix $\mathbf{G}_f$ is constructed such that: the external moment on the node located at the base of the first link is equal to the base motor torque, the moment on the node located at the tip of the first link is the negative of the elbow motor

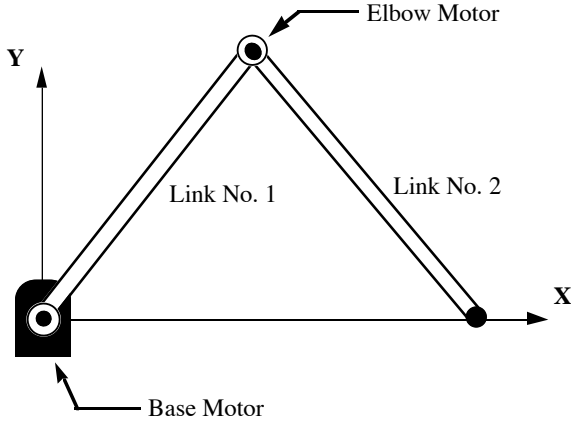

Figure 12.6. Open-chain planar multibody system.

torque, the external moment on the node located at the base of the second link is equal to the elbow motor torque, and all other external forces are zero.

Substituting equations (12.22) and (12.24) into (12.23) yields

$$\mathbf{m}_{ff}\ddot{\mathbf{q}}_f + \mathbf{c}_{ff}\dot{\mathbf{q}}_f + \mathbf{k}_{ff}\mathbf{q}_f = \mathbf{G}_f\mathbf{m}_{\theta f}\ddot{\mathbf{q}}_f + \mathbf{F}_1(\boldsymbol{\lambda}, \mathbf{q}_r, \dot{\mathbf{q}}_r, \ddot{\mathbf{q}}_r, \mathbf{q}_f, \dot{\mathbf{q}}_f) \tag{12.25}$$

where $\mathbf{F}_1$ is a force vector that includes the inertial terms, reaction terms between contiguous bodies, and quadratic velocity terms.

The problem statement for the inverse kinematics is that of finding the non-causal internal states $\mathbf{q}_f$ so that the endpoint coordinates characterized by a subset of the rigid body coordinates $\mathbf{q}_r$ follow a prescribed trajectory. The inverse kinematics equations (12.25) are nonlinear in the variable $\mathbf{q}_f$. As pointed out before, the nonlinear non-causal inversion cannot be carried out by standard numerical integration of ODEs. It requires a linearization process in either the frequency domain or time domain or splitting the linearized system into its causal and anti-causal components.

The key to the linearization process for the non-recursive approach relies on decomposing the inertial coupling submatrix $\mathbf{m}_{\theta f}$ into the sum of a time-invariant matrix and a time-varying matrix:

$$\mathbf{m}_{\theta f} = \mathbf{m}^c_{\theta f} + \mathbf{m}^t_{\theta f} \tag{12.26}$$

where the first and second components in the RHS are the time-invariant and the time-varying parts of $\mathbf{m}_{\theta f}$, respectively. This decomposition is essential for the iteration process needed to obtain the non-causal solution to the nonlinear inversion problem. Substituting (12.26) into (12.25), one can obtain the inverse kinematics equation of motion for the internal nodal displacements $\mathbf{q}_f$:

$$\mathbf{m}^*_{ff}\ddot{\mathbf{q}}_f + \mathbf{c}_{ff}\dot{\mathbf{q}}_f + \mathbf{k}_{ff}\mathbf{q}_f = \mathbf{F}(\boldsymbol{\lambda}, \mathbf{q}_r, \dot{\mathbf{q}}_r, \ddot{\mathbf{q}}_r, \mathbf{q}_f, \dot{\mathbf{q}}_f) \tag{12.27}$$

where

$$\mathbf{m}^*_{ff} = \mathbf{m}_{ff} - \mathbf{G}_f\mathbf{m}^c_{\theta f} \tag{12.28}$$

The mass matrix $\mathbf{m}^*_{ff}$ is non-symmetric. It is precisely the non-symmetry of the mass matrix that produces internal states $\mathbf{q}_f$ (nodal deformations). These states are non-causal with respect to the endpoint motion when non-causal techniques are employed to obtain the proper inversion of the nonlinear, non-minimum problem characterized by (12.27). The nonlinear inversion can now be carried out efficiently in the frequency domain, since the leading matrices have been constructed such that they remain constant throughout the motion. It is thus solved (12.27) iteratively in the frequency domain to yield the nodal deformation vector $\mathbf{q}_f$ that is non-causal with respect to the endpoint motion. Note that this iterative procedure is similar to that used in the recursive case. Each iteration can also be carried out in the time domain through the use of an equation similar to (12.17).

Once the non-causal nodal accelerations are known, equation (12.22) can be used to explicitly compute the non-causal inverse dynamics joint efforts. The inverse dynamics torques and internal states given by equations (12.22) and (12.25), respectively, depend on the Lagrange multipliers and rigid body coordinates which in turn depend on the internal states and the applied torque. The rigid

body coordinates and Lagrange multipliers are different from their normal values, when the components of the multibody system are flexible. Therefore, a forward dynamic analysis is required to obtain an improved estimate of the generalized coordinates and Lagrange multipliers. In order to ensure that the iteration process converges to obtain the joint efforts that will cause the end-effector to follow the desired trajectory, the forward dynamics analysis is carried out with the additional constraint that the coordinates of the endpoint follow the desired trajectory.

To summarize, the procedure for obtaining the inverse dynamics solution for flexible multibody systems involves the following steps:

Algorithm 12-5

1. Perform a rigid body inverse dynamic analysis to obtain the nominal values of the rigid body coordinates $\mathbf{q}_r$ and Lagrange multipliers $\boldsymbol{\lambda}$.
2. Solve the inverse kinematics equation (12.25), either in the frequency or time domain, to obtain the *non-causal* nodal accelerations $\ddot{\mathbf{q}}_f$
3. Compute the inverse dynamics joint efforts $\mathbf{Q}_{e\theta}$, using equation (12.22).
4. Perform a forward dynamic analysis, using equation (12.21) to obtain new values for the generalized coordinates and Lagrange multipliers.
5. Repeat steps 2 through 4 until convergence in the inverse dynamics torques is achieved.

Compare the recursive procedure and the non-recursive Lagrangian procedure for the inverse dynamics of multibody systems. In the former method, each body in the multibody system is analyzed sequentially, starting from the last element in the chain. For each element, the joint torques are determined first under the assumption that the rigid body coordinates are moving according to the nominal trajectory. With the joint actuation known for this component, a forward dynamic analysis is carried out for this component to determine the nodal deformations. The reaction forces from the next element in the chain are subsequently determined from equilibrium considerations. This recursive method works very well for open-chain systems but is not suitable for closed-chains. In these cases, the reaction forces at the cuts need to be accounted for by *ad hoc* procedures (Bayo et al. (1989)). The non-recursive method avoids this problem, since the reactions between different bodies are automatically accounted for by the Lagrange multipliers and no distinction is made between open-chain and closed-chain configurations. *The non-recursive procedure, although more involved, is therefore more systematic and general.*

12.3.1 A Planar Open-Chain Example

In order to illustrate the performance of the above-mentioned algorithms we describe in this section some results. Consider the system of Figure 12.6 which consists of two flexible aluminum links and two revolute joints driven directly

Figure 12.7. Tip acceleration profile.

by servo motors. The intention is to apply both the recursive and non-recursive approaches and compare the results to test their validity.

The links have the following characteristics:

First link: $L = 0.66$m, $A = 1.2097\text{x}10^{-4}$ m^2, $I = 2.2864\text{x}10^{-10}$ m^4, $M_t = 1.049$ Kg, $I_h = 0.0011823$ m^4

Second link: $L = 0.66$ m, $A = 0.4032\text{x}10^{-4}$ m^2, $I = 8.4683\text{x}10^{-12}$ m^4, $M_t = 0.067$ Kg, $I_h = 0.00048$ m^4

They both share the following properties: $E = 7.11\text{x}10^{10}$ N/m^2, mass density $\rho = 2715$ Kg/m^3, shear coefficient $k = 5/6$, and a damping ratio of 0.002. The cross section of the links is such that the arm is rigid in the vertical direction and flexible in the horizontal direction.

A straight-line tip trajectory along the x axis is generated according to the acceleration profile shown in Figure 12.7 which corresponds to an endpoint displacement of 0.483 meters. Optimal acceleration profiles for inverse dynamics have also been proposed (Bayo and Paden (1987), and Serna and Bayo (1990)).

Figure 12.8 shows the inverse dynamics torque profile for the base motor. Both the recursive and non-recursive methods yield the same results that superimpose to each other (solid curve). The inverse dynamics torque profiles for the elbow motor computed by both methods also coincide and are superimposed to each other in Figure 12.9 (solid curve). Therefore, it is a good validation to see that the results obtained are the same regardless of the method used. The corresponding rigid body torques which are torques obtained considering that the system is rigid are also shown as dashed curves in Figures 12.8 and 12.9 to clearly illustrate the pre-actuation present in the inverse dynamics torque profiles of the flexible system.

Figure 12.8. Rigid (dotted) and flexible (solid) inverse dynamics torques for first motor.

Figure 12.9. Rigid (dotted) and flexible inverse (solid) dynamics torques for second motor.

The inverse dynamics torques produce the desired tip trajectory *without overshoot or residual oscillations*. Figure 12.10 shows a comparison of the tip position error in the y direction resulting from feed forwarding the inverse dynamics torque (solid curve) and the rigid body torque (dashed curve). While the inverse dynamics torque provides an excellent tracking of the tip trajectory, the rigid torque induces a large oscillation in the tip motion. Figure 12.11 shows a com-

Figure 12.10. Tip error: inverse dynamic (solid) vs. rigid torques (dotted).

Figure 12.11. Elastic hub rotation: inverse dynamic (solid) vs. rigid torques (dotted).

parison of the elastic angular rotation at the base of the second link, obtained by a feed forward of the inverse dynamics torque (solid curve) to that obtained by a feed forward of the rigid body torque (dashed curve). One can observe that while the inverse dynamics torque does not induce residual vibration, the rigid body torque induces substantial residual oscillation.

A very important feature of the inverse dynamics is that not only the tip trajectory is tracked but also that the vibrations are minimized; so that the actual

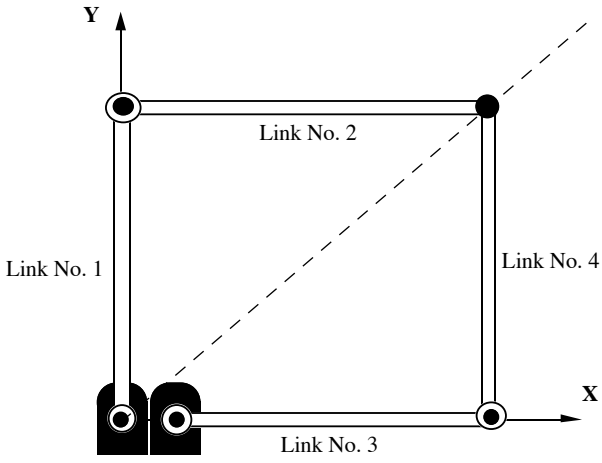

Figure 12.12. Closed-chain flexible multibody systems.

Figure 12.13. Rigid (dotted) and flexible inverse (solid) dynamics torques.

motion of the whole system resembles that of a rigid system (Bayo et al. (1988 and 1989)). An experimental validation consisting in feed forwarding the inverse dynamics torques to this flexible multibody system is presented in Bayo et al. (1989). An exponentially stable control scheme based on the inverse dynamics has been recently proposed and experimentally validated by Paden et al. (1993).

Figure 12.14. Tip error: inverse dynamic (solid) vs. rigid torques (dotted).

12.3.2 A Planar Closed-Chain Example

The non-recursive procedure can be applied to closed-chain configurations without loss of generality. For example, the inverse dynamics and kinematics are calculated for the closed-chain system depicted in the Figure 12.12. A straight-line tip trajectory along the diagonal (See Figure 12.12) is generated according to an acceleration profile similar to that of Figure 12.7. Figure 12.13 shows the inverse dynamics torque profile for one of the base motors. In this case, only the non-recursive method is applied, since the closed-loop configuration precludes the recursive procedure from a straightforward application. The corresponding rigid-body torque (torques obtained considering that the system is rigid) is also shown as a dashed curve in Figures 12.13 to again illustrate the pre-actuation present in the inverse dynamics torque profile of the flexible system.

Figure 12.14 shows a comparison of the tip position error in the y direction resulting from feed forwarding the inverse dynamics torque (solid curve) and the rigid body torque (dashed curve). While the inverse dynamics torque provides an excellent tracking of the tip trajectory, the rigid torque induces a large oscillation in the tip motion.

Appendix

We present in this Appendix the body matrices of equation (12.6) corresponding to a Timoshenko beam finite element. The axial deformation is modeled with linear element shapes defined by

$$N_1(x) = \frac{x}{L} \quad \text{and} \quad N_2(x) = 1 - \frac{x}{L}$$

and Hermite polynomials for the bending deformation are

$$H_1(x) = 1 - 3\left(\frac{x}{L}\right)^2 + 2\left(\frac{x}{L}\right)^3 \quad , \quad H_2(x) = x - 2L\left(\frac{x}{L}\right)^2 + L\left(\frac{x}{L}\right)^3$$

$$H_3(x) = 3\left(\frac{x}{L}\right)^2 - 2\left(\frac{x}{L}\right)^3 \quad , \quad H_4(x) = -L\left(\frac{x}{L}\right)^2 + L\left(\frac{x}{L}\right)^3$$

Element mass matrix

$$\frac{\overline{m}\,L}{420}\begin{bmatrix}
140 & 0 & 0 & 70 & 0 & 0 \\
0 & 156+504\frac{\eta^2}{L^2} & 22L+42\frac{\eta^2}{L} & 0 & 54-504\frac{\eta^2}{L^2} & -13L+42\frac{\eta^2}{L} \\
0 & 22L+42\frac{\eta^2}{L} & 4L^2+56\eta^2 & 0 & 13L-42\frac{\eta^2}{L} & -3L^2-14\eta^2 \\
70 & 0 & 0 & 140 & 0 & 0 \\
0 & 54-504\frac{\eta^2}{L^2} & 13L-42\frac{\eta^2}{L} & 0 & 156+504\frac{\eta^2}{L^2} & -22L-42\frac{\eta^2}{L} \\
0 & -13L+42\frac{\eta^2}{L} & -3L^2-14\eta^2 & 0 & -22L-42\frac{\eta^2}{L} & 4L^2+56\eta^2
\end{bmatrix}$$

Element centrifugal matrix

$$\frac{\overline{m}\,L}{420}\begin{bmatrix}
-140\,\omega_h^2 & -147\,\dot{\omega}_h & 21\,L\,\dot{\omega}_h & -70\,\omega_h^2 & -63\,\dot{\omega}_h & 14\,L\,\dot{\omega}_h \\
147\,\dot{\omega}_h & -156\,\omega_h^2 & -22\,L\,\omega_h^2 & 63\,\dot{\omega}_h & -54\,\omega_h^2 & 13\,L\,\omega_h^2 \\
-21\,L\,\dot{\omega}_h & -22\,L\,\omega_h^2 & -4\,L^2\,\omega_h^2 & 14\,L\,\dot{\omega}_h & -13\,L\,\omega_h^2 & 3\,L^2\,\omega_h^2 \\
-70\,\omega_h^2 & -63\,\dot{\omega}_h & -14\,L\,\dot{\omega}_h & -140\,\omega_h^2 & -147\,\dot{\omega}_h & 21\,L\,\dot{\omega}_h \\
63\,\dot{\omega}_h & -54\,\omega_h^2 & -13\,L\,\omega_h^2 & 147\,\dot{\omega}_h & -156\,\omega_h^2 & 22\,L\,\omega_h^2 \\
-14\,L\,\dot{\omega}_h & 13\,L\,\omega_h^2 & 3\,L^2\,\omega_h^2 & -21\,L\,\dot{\omega}_h & 22\,L\,\omega_h^2 & -4\,L^2\,\omega_h^2
\end{bmatrix}$$

The part of the element centrifugal matrix multiplying $\dot{\omega}_h$ is skew-symmetric, and the part multiplying ω_h^2 is symmetric.

Element Coriolis matrix

$$-\frac{2\,\overline{m}\,L\,\omega_h}{60}\begin{bmatrix} 0 & 21 & 3\,L & 0 & 9 & -2\,L \\ -21 & 0 & 0 & -9 & 0 & 0 \\ -3\,L & 0 & 0 & -2\,L & 0 & 0 \\ 0 & 9 & 2\,L & 0 & 21 & -3\,L \\ -9 & 0 & 0 & -21 & 0 & 0 \\ 2\,L & 0 & 0 & 3\,L & 0 & 0 \end{bmatrix}$$

The element Coriolis matrix is skew-symmetric.

Element stiffness matrix

$$\begin{bmatrix} \frac{EA}{L} & 0 & 0 & -\frac{EA}{L} & 0 & 0 \\ 0 & 12\,\frac{EI}{L^3} & 6\,\frac{EI}{L^2} & 0 & -12\,\frac{EI}{L^3} & 6\,\frac{EI}{L^2} \\ 0 & 6\,\frac{EI}{L^2} & 4\,\frac{EI}{L} & 0 & -6\,\frac{EI}{L^2} & 2\,\frac{EI}{L} \\ -\frac{EA}{L} & 0 & 0 & \frac{EA}{L} & 0 & 0 \\ 0 & -12\,\frac{EI}{L^3} & -6\,\frac{EI}{L^2} & 0 & 12\,\frac{EI}{L^3} & -6\,\frac{EI}{L^2} \\ 0 & 6\,\frac{EI}{L^2} & 2\,\frac{EI}{L} & 0 & -6\,\frac{EI}{L^2} & 4\,\frac{EI}{L} \end{bmatrix}$$

Element force vector

$$\frac{\overline{m}\,L^2}{60}\begin{Bmatrix} 10\,\omega_h^2\,(1+3\,\frac{d}{L}) \\ -\dot{\omega}_h\,(9+30\,\frac{d}{L}) \\ -\dot{\omega}_h\,(2\,L+5\,d) \\ 10\,\omega_h^2\,(2+3\,\frac{d}{L}) \\ -\dot{\omega}_h\,(21+30\,\frac{d}{L}) \\ -\dot{\omega}_h\,(-3\,L-5\,d) \end{Bmatrix}$$

References

Bathe, K.-J., *Finite Element Procedures in Engineering Analysis*, Prentice-Hall, (1982).

Bayo, E., "A Finite Element Approach to Control the End-Point Motion of a Single Link Flexible Robot", *Journal of Robotic Systems*, Vol. 4, pp. 63-75, (1987).

Bayo, E. and Paden, B., "On Trajectory Generation of Flexible Robots", *Journal of Robotic Systems*, Vol. 4, pp. 229-235, (1987).

Bayo, E., Movaghar, R., and Medus, M., "Inverse Dynamics of a Single-Link Flexible Robot. Analytical and Experimental Results", *International Journal of Robotics and Automation*, Vol. 3, pp. 150-157, (1988).

Bayo, E. and Moulin, H., "An Efficient Computation of the Inverse Dynamics of Flexible Manipulators in the Time Domain", *Proceedings of the 1989 IEEE Conference on Robotics and Automation*, Vol. 2, pp. 710-715, Scottsdale, Arizona, (1989a).

Bayo, E. and Moulin, H., "Stiffening Effects in the Inverse Dynamics of Flexible Manipulators", in *Robotics Research – 1989*, pp. 161-167, edited by Y. Youcef-Touni and H. Kazerooni, ASME Press, (1989b).

Bayo, E., Serna, M.A., Papadopoulos, P., and Stubbe, J.R., "Inverse Dynamics and Kinematics of Multi-Link Elastic Robots: An Iterative Frequency Domain Approach", *The International Journal of Robotics Research*, Vol. 8, pp. 49-62, (1989).

Greenwood, T.J., *Principles of Dynamics*, 2nd edition, Prentice-Hall, (1988).

Kwon, D.S. and Book, W., "An Inverse Dynamic Method Yielding Flexible Manipulator State Trajectory", *Proceedings of the 1990 ACC Conference*, Vol. 1, pp. 186-193, (1990).

Ledesma, R. and Bayo, E., "A Non-recursive Lagrangian Approach for the Non-causal Inverse Dynamics of Flexible Multibody Systems. The Planar Case", Report # UCSB-ME-92-2, Mechanical Engineering Department, University of California, Santa Barbara, CA 93106, (1992a). Also to appear in the *International Journal of Numerical Methods in Engineering*, Vol. 36, (1993).

Ledesma, R. and Bayo, E., "Inverse Dynamics of Spatial Flexible Manipulators with Lumped and Distributed Actuators", Report # UCSB-ME-92-4 Mechanical Engineering Department. University of California. Santa Barbara, CA 93106, (1992b).

Ledesma, R. and Bayo, E., "A Non-recursive Lagrangian Approach for the Non-Causal Inverse Dynamics of Flexible Multibody Systems. The Spatial Case", Report # UCSB-ME-93-2, Mechanical Engineering Department, University of California, Santa Barbara, CA 93106, (1993).

Moulin, H., "Problems in the Inverse Dynamics Solution for Flexible Manipulators", Ph.D. Dissertation, University of California, Santa Barbara, (1989).

Moulin, H. and Bayo, E., "On the End-Point Trajectory Tracking for Flexible Manipulators through Non-Causal Inverse Dynamics", *ASME Journal of Dynamic Systems, Measurement, and Control*, Vol. 113, pp. 320-324, (1991).

Moulin, H., Bayo, E., and Paden, B., "Existence and Uniqueness of Solutions of the Inverse Dynamics of Multi-Link Flexible Arms. Convergence of a Numerical Scheme", *Journal of Robotic Systems*, Vol. 10, pp. 73-102, (1993).

Newland, D.E., *An Introduction to Random Vibrations and Spectral Analysis. Second Edition,* Longman, (1984).

Paden, B., Bayo, E., Dagang, C., and Ledesma, R. "Exponentially Stable Tracking Control for Multi-Joint Flexible-Link Manipulators", *ASME Journal of Dynamic Systems, Measurement, and Control*, Vol. 115, pp. 53-60, (1993).

Serna, M.A. and Bayo, E., "Off-Line Trajectory Planning for Flexible Manipulators", in *Modelling the Innovation: Communications, Automation and Information Systems*, Elsevier Science Publishers, pp. 213-220, (1990).